JOURNAL OF SYNCHROTRON RADIATION

ISSN 1600-5775

Received 18 July 2016
Accepted 3 October 2016

Edited by V. Favre-Nicolin, CEA and Université Joseph Fourier, France

Keywords: silicon wafer surface; total reflection X-ray fluorescence; Cu nanoparticle; grazing-incidence X-ray fluorescence.

Supporting information: this article has supporting information at journals.iucr.org/s

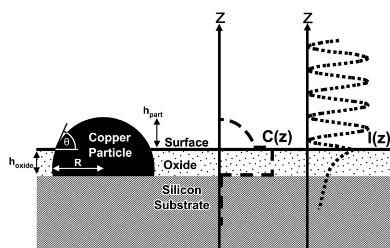

© 2017 International Union of Crystallography

Determination of copper nanoparticle size distributions with total reflection X-ray fluorescence spectroscopy

Andy Singh,[a] Katharina Luening,[a] Sean Brennan,[a] Takayuki Homma,[b] Nobuhiro Kubo,[b] Stanisław H. Nowak[a] and Piero Pianetta[a]*

[a]Stanford Synchrotron Radiation Laboratory, 2575 Sand Hill Road, Stanford, CA 94025, USA, and [b]Department of Applied Chemistry, Waseda University, Shinjuku, Tokyo 169-8555, Japan. *Correspondence e-mail: pianetta@slac.stanford.edu

Total reflection X-ray fluorescence (TXRF) analysis is extensively used by the semiconductor industry for measuring trace metal contamination on silicon surfaces. In addition to determining the quantity of impurities on a surface, TXRF can reveal information about the vertical distribution of contaminants by measuring the fluorescence signal as a function of the angle of incidence. In this study, two samples were intentionally contaminated with copper in non-deoxygenated and deoxygenated ultrapure water (UPW) resulting in impurity profiles that were either atomically dispersed in a thin film or particle-like, respectively. The concentration profile of the samples immersed into deoxygenated UPW was calculated using a theoretical concentration profile representative of particles, yielding a mean particle height of 16.1 nm. However, the resulting theoretical profile suggested that a distribution of particle heights exists on the surface. The fit of the angular distribution data was further refined by minimizing the residual error of a least-squares fit employing a model with a Gaussian distribution of particle heights about the mean height. The presence of a height distribution was also confirmed with atomic force microscopy measurements.

1. Introduction

Contamination analysis of silicon wafer surfaces with total reflection X-ray fluorescence (TXRF) has been critical for understanding and improving silicon processing technologies (Pahlke, 2003; Hockett, 1994; Pahlke *et al.*, 2001; Pianetta *et al.*, 1995). With the continuing drive to increase device density, the acceptable levels of surface contamination have been decreasing requiring transition metal impurity levels on silicon surfaces to be in the low 10^9 atoms cm^{-2} range (Kern, 2008; Hoefflinger, 2011). With TXRF, wafer surfaces can be measured non-destructively and detection limits of the order of 5×10^9 atoms cm^{-2} for various transition metals have been routinely achieved with conventional X-ray sources (Klockenkämper & von Bohlen, 2014). Even better sensitivities can be achieved with the use of vapor phase decomposition (VPD) techniques (Yamagami *et al.*, 1999). Moreover, by using synchrotron radiation sources, these detections limits have been greatly enhanced to levels of 8×10^7 atoms cm^{-2} due to the high flux density (Pianetta *et al.*, 2000).

In addition to measuring surface concentrations, geometrical information on the vertical distribution of contaminants can be determined by using the TXRF technique in the so-called grazing-incidence X-ray fluorescence (GIXRF) mode, where the fluorescence signal of an impurity is monitored as

a function of the angle of incidence (Klockenkämper & von Bohlen, 2014; Meirer *et al.*, 2010). For example, it is possible to ascertain whether contaminants are atomically dispersed throughout the bulk, incorporated in a thin film layer or exist as particles above the surface. This is the result of a standing wave pattern that is formed directly above the silicon surface due to interference between the incoming X-ray beam and the totally reflected beam. The periodicity of these standing waves, as well as the penetration depth of the X-rays, can be modulated by changing the angle of incidence. Therefore, the fluorescence intensity as a function of angle will strongly depend on the vertical distribution of the element of interest.

In fact, quantitative analysis to determine the vertical concentration profile of an impurity can be carried out through the use of least-squares fitting provided an accurate model for the concentration profile is used (Schwenke *et al.*, 1997). Such studies have proven useful in conducting depth profiles of ions implanted in Si and Ge (Hönicke *et al.*, 2012; Kayser *et al.*, 2015), and also in characterization of surface particles (Nowak *et al.*, 2013; Reinhardt *et al.*, 2012). In this study, a similar analysis was carried out in order to determine the mean particle height of Cu particles deposited in deoxygenated ultrapure water (UPW). In addition, through the use of atomic force microscopy (AFM) measurements, it was found that a height distribution of particles existed. By refining the model describing the Cu concentration profile to account for the particle height distribution, it was possible to improve the fit and extract additional parameters, such as the width of the distribution, from the GIXRF measurements.

2. Experimental

Cleaved 20 mm × 10 mm Si wafers were cleaned using a 4:1 sulfuric acid/hydrogen peroxide mixture (H_2SO_4 = 96 vol.%; H_2O_2 = 30 vol.%) for 10 min and then rinsed in deoxygenated UPW. Then they were dipped for 1 min into a 0.5% HF solution resulting in a clean hydrogen-terminated surface. The influence of oxygen in the UPW was studied by comparing the results from solutions made using standard UPW containing 3–10 p.p.m. of dissolved O_2 with those made using deoxygenated UPW solutions, prepared by sparging with argon, in which the dissolved O_2 content was reduced to approximately 0.3 p.p.m. The O_2 level in standard UPW was estimated from separate XPS measurements of the oxidation rate of a Si wafer when placed in UPW (Kasnavi *et al.*, 2001) and then compared with literature values of oxidation rate *versus* UPW O_2 concentration (Yagi *et al.*, 1992; Li *et al.*, 2005). The O_2 level in the deoxygenated UPW was estimated from literature values of studies using a similar sparging procedure (Li *et al.*, 2005; Butler *et al.*, 1994). Copper in a 2% nitric acid matrix was then introduced at concentration levels of 100 p.p.b. and the Si surfaces were contaminated by immersing the hydrogen-terminated silicon samples into these solutions for 300 s.

The surface concentration of the copper contaminants was analyzed using SR-TXRF on the 6-2 beamline at the Stanford Synchrotron Radiation Laboratory (SSRL) at an incident beam energy of 11.2 keV. In order to determine if the Cu was deposited as a thin surface layer or as particles on the Si surfaces, the Cu fluorescence signal was measured as a function of incident beam angle from 0.01 to 0.3°. In the sample where the copper was as nanoparticles, AFM measurements were also taken to confirm the particle size distribution. Further details on the sample preparation and experimental setup are discussed elsewhere (Singh *et al.*, 2004; Pianetta *et al.*, 2000).

3. Results and discussion

Fig. 1 shows the Cu fluorescence intensity as a function of the angle of incidence for samples immersed in 100 p.p.b. Cu-contaminated UPW solutions. As can be seen, the sample prepared in non-deoxygenated UPW has a profile indicative of atomically dispersed Cu near the surface, where the maximum in fluorescence intensity occurs at the critical angle of 0.16°. On the other hand, the sample immersed in deoxygenated UPW has a fluorescence maximum at 0.1°, suggesting that Cu particles are present on the surface.

For the samples immersed in deoxygenated UPW, a model depicting the vertical concentration profile is shown in Fig. 2. Here Cu particles grow as spherical caps extending beneath a thin oxide layer terminating at the silicon surface. Additional atomic Cu is incorporated into the native oxide that readily grows in deoxygenated UPW. Above the oxide surface, Cu only exists as metallic particles. In this region, the Cu concentration is determined by the mean height and the mean contact angle of the Cu particles. Therefore, a total of four parameters specify the concentration profile: (1) the height of the oxide, (2) the ratio between Cu surface concentration in the particle just above the oxide surface and the Cu surface concentration in the oxide layer, (3) the particle height and (4) the contact angle of the particle. In the oxide the amount of atomically dispersed Cu is much higher than the metallic Cu from the particles that terminate at the silicon surface, and, consequently, the concentration of Cu in the oxide can be assumed to be constant and independent of height. Mathe-

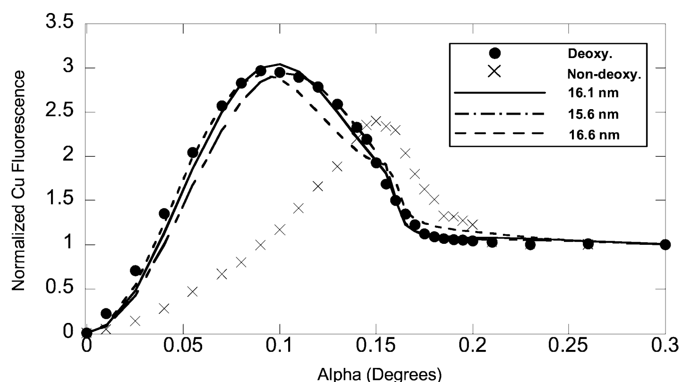

Figure 1
Fluorescence intensity *versus* angle of incidence for samples immersed in deoxygenated and non-deoxygenated UPW solutions containing 100 p.p.b. Cu. The critical angle for silicon is at 0.16°. A least-squares fit using a specific concentration profile yielded a particle height of 16.1 nm. Additional calculations for particles of height 15.6 and 16.6 nm are shown. Reproduced with permission from Singh (2004).

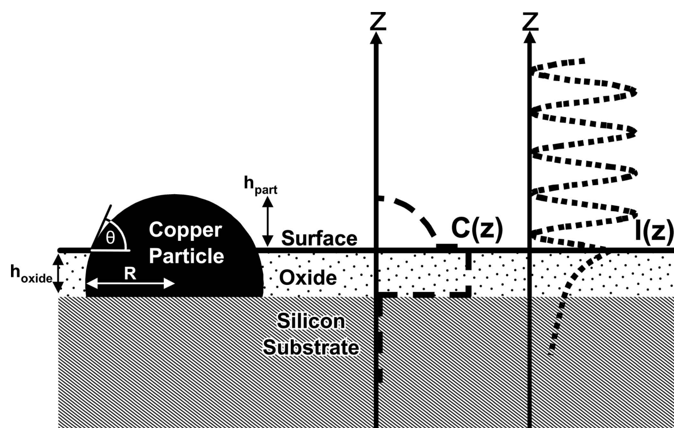

Figure 2
Model for the concentration profile used in the least-squares fits. The stitched line (– – –) shows the concentration profile, $c(z)$, and the dashed line (-----) shows the corresponding intensity profile, $I(z)$.

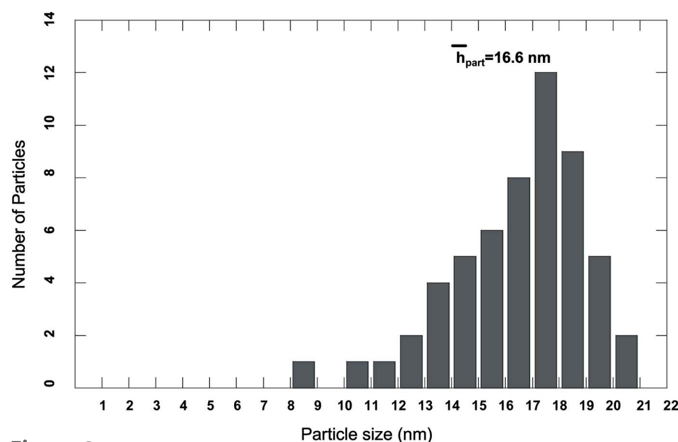

Figure 3
Particle size distribution of a sample immersed in deoxygenated UPW for 5 min containing 100 p.p.b. Cu as measured using AFM. The scan area of the sample was 20 µm × 20 µm. As can be seen the mean particle height of 16.6 nm agrees well with fits performed on fluorescence signal *versus* angle measurements.

matically, the concentration profile used is expressed as shown:

$$X_{\rm Cu}(z) = 1 \qquad \text{for } 0 \le z \le h_{\rm oxide},$$
$$X_{\rm Cu}(z) = \kappa A_{\rm cap}(\theta, R, z)/V_{\rm cap}(\theta, R) \qquad \text{for } z > h_{\rm oxide},$$

where $X_{\rm Cu}$ is the relative copper concentration, z is the height above the silicon/oxide interface, $h_{\rm oxide}$ is the height of the oxide layer, κ is the ratio of the quantity of copper in the particle and the quantity of copper in the oxide, $A_{\rm cap}$ is the cross-sectional area of the Cu particle, $V_{\rm cap}$ is the particle volume, θ is the contact angle and R is the radius of the spherical cap.

For reference, a schematic of the standing wave intensity profile is also shown in Fig. 2; however, the overall profile changes with the angle because the frequency of the standing waves that form above the surface and the penetration depth of the X-ray into the sample both increase with the angle. The relative fluorescence signal at a specific angle can be simulated by multiplying the concentration profile with the intensity profile and integrating this product over the full spatial range of the copper. A least-squares fit of the Cu GIXRF intensity profile was then performed for the sample immersed in deoxygenated UPW.

For the sample contaminated in deoxygenated UPW the results of the least-squares fit indicate the presence of nanoparticles with a mean height of 16.1 nm, a contact angle of 59° and a concentration ratio of 0.027; the oxide thickness was found to be 0.52 nm. Additional model calculations assuming 15.6 and 16.6 nm particles are also shown in Fig. 1 to demonstrate the precision of this technique. As can be seen, the 16.6 nm fit shows better agreement with the data at angles below 0.09°, whereas the 15.6 nm fit better corresponds to the data at higher angles above 0.11°. From these additional results, it can be inferred that a range of particles with differing sizes exist on the surface, because larger (smaller) particles would exhibit greater fluorescence intensity at smaller (larger) angles.

In order to confirm that a range of particle sizes does exist, AFM measurements were conducted on the sample that was immersed in deoxygenated UPW (AFM images can be found in the supporting information). From these measurements, it was possible to extract a particle height distribution, which is shown in Fig. 3. As can be seen, a range of particle heights exists in a Gaussian-like distribution that is skewed towards higher particles. From this distribution, the mean particle height was determined to be 16.6 nm, which was approximately 0.5 nm greater than the value extracted from the least-squares fit conducted on the fluorescence signal data shown in Fig. 1.

In Fig. 4, the measured Cu fluorescence intensity is plotted as a function of angle for the sample immersed in 100 p.p.b. Cu-contaminated deoxygenated UPW solutions along with the same least-squares fit that was shown in Fig. 1. Additionally, the theoretical fluorescence curve using the particle height distribution shown in Fig. 3 was also plotted. In order to perform this calculation, the concentration profile was calculated by taking a weighted average of the distribution of

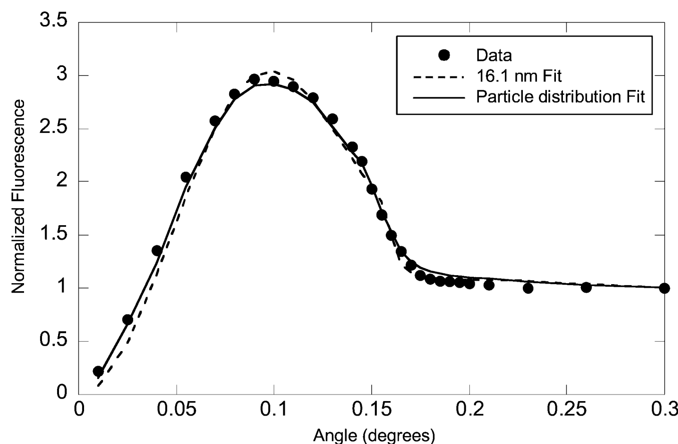

Figure 4
Using the distribution of particle sizes shown in Fig. 3, the theoretical fluorescence signal *versus* incident beam angle was plotted. Compared with the 16.1 nm fit shown in Fig. 1, the profile is broader and overall is a better fit.

the different particle heights as obtained from the AFM measurements. As can be seen, several noticeable differences between the theoretical fluorescence using the distribution of particle height and the original least-squares fit using a single particle size are apparent. Firstly, the figure shows that a better fit to the data is achieved at lower angles when using the distribution of particle sizes. As larger particles have a maximum in fluorescence intensity at smaller angles, it is expected that the theoretical fluorescence calculated when using a distribution of particles is greater at small angles. Secondly, it can also be seen that a greater amount of fluorescence is predicted at large angles when the distribution of particles is used. In this case, the smaller particles in the distribution contribute to the predicted fluorescence intensity at large angles. Finally, it can be seen that the maximum in fluorescence intensity when using the distribution of particles is less when using particles of the same size. With regards to the data, neither profile exhibits a better fit in the region near the fluorescence intensity maximum, as calculations using the distribution of particles are too low, whereas the fit using particles of the same height is too high. However, when examining both profiles over the full range of data, it is clear that the calculation using the distribution of particles more accurately corresponds to the data.

In order to demonstrate that GIXRF itself is a technique sensitive enough to also provide information on the particle distribution, another least-squares fit was conducted on the experimental data. In this fit, a Gaussian particle height distribution about a mean of 16.1 nm was used to describe the concentration profile. In Fig. 5, the residual error of this calculation is shown as a function of the full-width at half maximum (FWHM) of the particle height distribution. From this plot, it can be seen that the quality of the fit improves by assuming that a distribution of particle heights exist. Assuming that all particles have the same height, as was done for the fit shown in Fig. 1, the residual error is approximately 2.60 as can be seen in Fig. 5. However, with increasing FWHM, the residual drops to lower values until reaching a minimum value when FWHM is 2.8 nm. This value of 2.8 nm corresponds well to the FWHM extracted from the AFM measurements, which was determined to be 3.8 nm. The difference between these results can most likely be attributed to the fact that the actual profile measured with AFM is a skewed distribution such that a tail exists on the lower particle height side of the distribution, which was not modeled when performing the least-squares fit with the Gaussian distribution. Furthermore, the minimum is broad and a change in the FWHM value of $\pm$2.0 nm only increases the residual error by 3.5%. However, the residual error of the fit clearly improves by using a Gaussian distribution and indicates that depth profiling in the TXRF geometry is a technique sensitive enough to detect the difference between particles that all have the same height and those that exist as a distribution of heights.

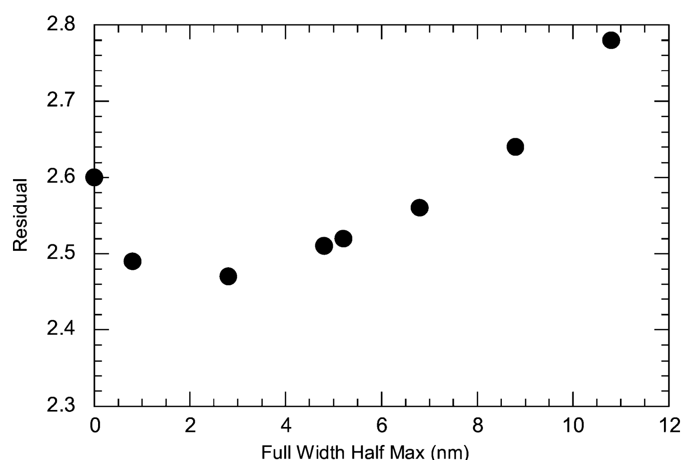

Figure 5
The residual error is shown as a function of FWHM for a number of fits performed using the Gaussian distribution to model the concentration profile of particles. As can be seen, the best fit occurs at approximately 2.8 nm.

4. Conclusion

In conclusion, it was demonstrated that measuring the fluorescence intensity *versus* the angle of incidence for samples with particle-like contaminants grown on the surface can yield quantitative information, although the choice of the concentration profile can subtly change the results. In this study, when using a concentration profile representative of particles of all the same height, the resulting least-squares fit to the fluorescence signal angle scan showed significant differences to the data measured, especially at smaller angles. However, by using a concentration profile that took a weighted average of a distribution of particles, as determined *via* AFM measurements, it was found that the predicted theoretical fluorescence more accurately corresponded to the data. Finally, it was possible to obtain the particle height distribution directly from the GIXRF data by adding a Gaussian particle height distribution to the model and using a least-squares fit to minimize the residual error resulting in a particle height distribution of 2.8 nm. By identifying the nature of the contaminants on silicon wafer surfaces, it should be possible to better determine and eliminate the source of processing issues when they arise in the semiconductor fabrication plant.

Acknowledgements

We would like to thank the staff at SSRL for their expert technical assistance. This work was performed at SSRL, which is supported by the Department of Energy, Office of Basic Energy Sciences. The support of SIWEDS is also acknowledged. SHN acknowledges support from the Swiss National Science Foundation (SNSF), project No. 148569.

References

Butler, I. B., Schoonen, M. A. A. & Rickard, D. T. (1994). *Talanta*, **41**, 211–215.
Hockett, R. S. (1994). *MRS Online Proc. Libr. Arch.* **354**, 377.
Hoefflinger, B. (2011). Editor. *Chips 2020: A Guide to the Future of Nanoelectronics*, pp. 161–174. Berlin, Heidelberg: Springer.

Hönicke, P., Kayser, Y., Beckhoff, B., Müller, M., Dousse, J.-C., Hoszowska, J. & Nowak, S. H. (2012). *J. Anal. At. Spectrom.* **27**, 1432–1438.

Kasnavi, R., Sun, Y., Mount, G., Pianetta, P., Griffin, P. B. & Plummer, J. D. (2001). *Electrochem. Solid-State Lett.* **4**, G1–G3.

Kayser, Y., Hönicke, P., Banaś, D., Dousse, J.-C., Hoszowska, J., Jagodziński, P., Kubala-Kukuś, A., Nowak, S. H. & Pajek, M. (2015). *J. Anal. At. Spectrom.* **30**, 1086–1099.

Kern, W. (2008). *Handbook of Silicon Wafer Cleaning Technology*, pp. 3–92. Amsterdam: Elsevier.

Klockenkämper, R. & von Bohlen, A. (2014). *Total-Reflection X-ray Fluorescence Analysis and Related Methods.* New York: Wiley.

Li, F., Balazs, M. K. & Anderson, S. (2005). *J. Electrochem. Soc.* **152**, G669.

Meirer, F., Singh, A., Pianetta, P., Pepponi, G., Meirer, F., Streli, C. & Homma, T. (2010). *Trends Anal. Chem.* **29**, 479–496.

Nowak, S. H., Reinhardt, F., Beckhoff, B., Dousse, J.-C. & Szlachetko, J. (2013). *J. Anal. At. Spectrom.* **28**, 689–696.

Pahlke, S. (2003). *At. Spectrosc.* **58**, 2025–2038.

Pahlke, S., Fabry, L., Kotz, L., Mantler, C. & Ehmann, T. (2001). *At. Spectrosc.* **56**, 2261–2274.

Pianetta, P., Baur, K., Singh, A., Brennan, S., Kerner, J., Werho, D. & Wang, J. (2000). *Thin Solid Films*, **373**, 222–226.

Pianetta, P., Takaura, N., Brennan, S., Tompkins, W., Laderman, S. S., Fischer-Colbrie, A., Shimazaki, A., Miyazaki, K., Madden, M., Wherry, D. C. & Kortright, J. B. (1995). *Rev. Sci. Instrum.* **66**, 1293–1297.

Reinhardt, F., Beckhoff, B., Pollakowski, B., Kolbe, M., Osán, J., Török, S., Schoengen, M., Nowak, S., Dousse, J.-C., Bresch, H., Seeger, S. & Waldschläger, U. (2012). *Proceedings of the European Conference on X-ray Spectrometry (EXRS 2012)*, 18–22 June 2012, Vienna, Austria.

Schwenke, H., Knoth, J., Fabry, L., Pahlke, S., Scholz, R. & Frey, L. (1997). *J. Electrochem. Soc.* **144**, 3979–3983.

Singh, A. (2004). PhD thesis, Stanford University, USA.

Singh, A., Luening, K., Brennan, S., Homma, T., Kubo, N. & Pianetta, P. (2004). *AIP Conf. Proc.* **705**, 1086–1089.

Yagi, Y., Imaoka, T., Ksama, Y. & Ohmi, T. (1992). *IEEE Trans. Semicond. Manuf.* **5**, 121–127.

Yamagami, M., Nonoguchi, M., Yamada, T., Shoji, T., Utaka, T., Nomura, S., Taniguchi, K., Wakita, H. & Ikeda, S. (1999). *X-ray Spectrom.* **28**, 451–455.